Journal of Materials Chemistry C

PAPER

View Article Online
View Journal | View Issue

Cite this: J. Mater. Chem. C, 2018, 6, 7249

Cu_2O@PNIPAM core–shell microgels as novel inkjet materials for the preparation of CuO hollow porous nanocubes gas sensing layers†

He Jia,[a] Haitao Gao,[b] Shilin Mei,[a] Janosch Kneer,[b] Xianzhong Lin,[c] Qidi Ran,[a] Fuxian Wang,[d] Stefan Palzer[e] and Yan Lu *[af]

Received 26th April 2018,
Accepted 18th June 2018

DOI: 10.1039/c8tc01995a

rsc.li/materials-c

There has been long-standing interest in developing metal oxide-based sensors with high sensitivity, selectivity, fast response and low material consumption. Here we report for the first time the utilization of Cu_2O@PNIPAM core–shell microgels with a nanocube-shaped core structure for construction of novel CuO gas sensing layers. The hybrid microgels show significant improvement in colloidal stability as compared to native Cu_2O nanocubes. Consequently, a homogeneous thin film of Cu_2O@PNIPAM nanoparticles can be engineered in a quite low solid content (1.5 wt%) by inkjet printing of the dispersion at an optimized viscosity and surface tension. Most importantly, thermal treatment of the Cu_2O@PNIPAM microgels forms porous CuO nanocubes, which show much faster response to relevant trace NO_2 gases than sensors produced from bare Cu_2O nanocubes. This outcome is due to the fact that the PNIPAM shell can successfully hinder the aggregation of CuO nanoparticles during pyrolysis, which enables full utilization of the sensor layers and better access of the gas to active sites. These results point out great potential of such an innovative system as gas sensors with low cost, fast response and high sensitivity.

Introduction

Semiconducting metal oxide-based gas sensors currently constitute one of the most investigated gas detection technologies due to their low cost, low power consumption, simple construction, and a broad range of detectable gases.[1–4] With the aim of enhancing sensitivity, selectivity, and response time, numerous efforts have been made to synthesize metal oxide nanostructures with high porosity, large surface area and a rich number of active sites.[5,6] In addition to the emphasis on morphology, the preservation of the defined nanostructures against transformation or deformation during manufacture have also attracted remarkable attention, which is essential to fully utilize the sensing layers and minimize the cost. However, achieving co-benefits of less material consumption, fast response, and higher sensitivity and selectivity has been an enduring challenge due to much less focus on the stabilization of semiconducting metal oxide nanoparticles, which is particularly important for the application of environmentally sensitive metal oxides such as Cu_2O.

Cu_2O is a well-known p-type semiconductor, which has been widely applied in photocatalytic degradation of dye molecules,[7–9] solar energy conversion,[10] lithium-ion batteries[11,12] and gas sensors.[13,14] It can be also used as precursor particles for fabricating CuO materials.[15] Due to the possibility to achieve highly selective detection of the toxic gas using Cu_2O and CuO as sensing material, both Cu_2O and CuO are of great interest in material research.[16–18] Consequently, the deposition of Cu_2O nanoparticles onto various substrates is of great importance in the construction of gas sensors, which has significant impact on the performance of the sensing layers.[19,20] Among the plethora of possible deposition techniques for nanostructures,[21] inkjet printing stands out as a flexible and scalable backend production process of functional layers. Inkjet printing has been one of the most effective deposition techniques due to its numerous advantages, such as economic use of functional materials, superior control of film thickness in nano-/micro-scale, and its

[a] Soft Matter and Functional Materials, Helmholtz-Zentrum Berlin für Materialien und Energie, Hahn-Meitner-Platz 1, Berlin, Germany. E-mail: yan.lu@helmholtz-berlin.de
[b] Laboratory for Gas Sensors, Department of Microsystems Engineering – IMTEK, University of Freiburg, Georges-Köhler-Allee 102, Freiburg, Germany
[c] Heterogeneous Materialien und Energie, Helmholtz-Zentrum Berlin für Materialien und Energie, Hahn-Meitner-Platz 1, Berlin, Germany
[d] Institute for Solar Fuels, Helmholtz-Zentrum Berlin für Materialien und Energie GmbH, 14109 Berlin, Germany
[e] Department of Computer Science, Universidad Autónoma de Madrid, Francisco Tomás y Valiente 11, 28049 Madrid, Spain
[f] Institute of Chemistry, University of Potsdam, 14467 Potsdam, Germany

† Electronic supplementary information (ESI) available. See DOI: 10.1039/c8tc01995a

feasibility to fabricate high quality patterns onto both hard and flexible substrates in a large volume production as well as in small batches.[22] Moreover, a combination of inkjet printing technology with so-called hotplate devices allows for quickly testing novel nano-sized gas sensitive materials.[15,23–25]

The strict requirements for the properties of the ink system top the list of challenges needed to be overcome for inkjet printing of Cu_2O nanoparticles. On the one hand, the stability of the ink system should meet the requirement to attain monodispersed patterns on the substrates without aggregation and can be long-term stored without deterioration. On the other hand, in order to obtain high resolution of the printed patterns, the viscosity and surface tension of the ink should be beneficial to minimize the size of the droplets according to Fromm's theory developed in 1984.[26,27,42]

Unfortunately, Cu_2O nanoparticles typically exhibit low environmental stability in water and the nanostructures are easily destroyed in an oxidation process. Thus, currently it remains hard to prepare inks with Cu_2O nanoparticles to meet all of the above requirements. Kim *et al.*[28] and Lee *et al.*[29] tried to stabilize Cu_2O nanoparticles in an aqueous solvent mixed with isopropanol or glycerol respectively, to improve the viscosity and surface tension of the ink. But the stability of Cu_2O individuals did not change significantly. Dasgupta *et al.*[30] chose sodium salt of poly(acrylic acid) (PAANa) as the stabilizer to prevent the oxidation of Cu_2O nanoparticles ink solution. Due to the adsorption of PAANa ligands, the surface energy of the nanoparticles was reduced resulting in a reduced tendency for agglomeration. Yang *et al.*[31] used oleic acid to stabilize Cu_2O nanoparticles and dispersed the samples into non-polar solvent instead of water to slow down the process of oxidation. In spite of these efforts, these reported methods can only extend the shelf life of the Cu_2O ink solution to a couple of weeks. Although efforts have been continuously made to improve the properties of Cu_2O nanoparticle ink solution, there is no effective method to be presented until now.

As one of the most well-known thermosensitive microgels, poly(*N*-isopropylacrylamide) (PNIPAM) has been used to modify different kinds of inorganic nanoparticles. Due to the hydrophilic property below the lower critical solution temperature (LCST), PNIPAM shells can increase the colloidal stability of nanoparticles in aqueous solution and help form an array with distance between each of the hybrid nanoparticles when they are dried on different substrates.[32–38] For instance, Liz-Marzán *et al.*[39] and Karg *et al.*[40] successfully synthesized hybrid systems by encapsulating gold and silver nanoparticles inside PNIPAM shells, respectively. Due to the modification of the PNIPAM shell, the colloidal stability of the nanoparticles was improved and the monolayer arrays of the particles can be obtained. Moreover, after removal of the PNIPAM shells by annealing at 700 °C, a monolayer of well-separated gold nanoparticles can still be retained.[40] Recently, we first applied this system to the p-type semiconductors, Cu_2O nanocubes. The colloid stability of the Cu_2O nanocubes have been enhanced significantly after PNIPAM coating and the PNIPAM shell can protect the Cu_2O nanocubes from fast oxidation for several months.[41]

Here we present for the first time the use of Cu_2O@PNIPAM core–shell nanoparticles as a novel ink system for the preparation of gas sensor device by inkjet printing technique. With the protection of the PNIPAM shells, the storage time of Cu_2O nanoparticles based ink solution was significantly prolonged, which can be kept for at least 3 months without oxidation. At the same time, the colloidal stability of the ink solution was obviously enhanced. The ink solution remained stable after standing overnight and can easily be redispersed homogeneously before inkjet printing after storing for several months, which guarantees homogeneous deposition. Moreover, Cu_2O@PNIPAM aqueous ink solution with low solid content (1.5 wt%) can meet the requirements for obtaining high resolution printed patterns according to Fromm's theory[42] without introducing any other surfactant and solvent.

The procedure for the preparation of gas sensor device by inkjet printing with Cu_2O@PNIPAM core–shell nanoparticles as the ink material was shown in Scheme 1. Assisted by PNIPAM shells, a homogeneous thin layer of Cu_2O@PNIPAM core–shell nanoparticles was obtained, which allows for the construction of multi-layers of Cu_2O@PNIPAM devices by repeating the inkjet printing process. Most importantly, after thermal treatment, a gas sensing layer consisting of CuO porous hollow nanocubes was formed and a well-defined space between adjacent CuO nanocubes has been achieved, which significantly increased the specific surface area of the sensing layer and improved the response time of the gas sensor device. The present approach can be easily extended to other functional nanoparticles and it allows for the preparation of gas sensor devices in a more environmentally friendly way by using much less materials. The results obtained with CuO nanocubes here is an addition to the results regarding the shape dependence of both sensitivity and selectivity of gas sensitive layers. The latter is particularly interesting for potential use of layers in real-world applications outside the laboratory, where the response characteristics of various metal-oxide based layers are employed for the so-called electronic noses.[43,44]

Previous results on CuO-based layers include studies of the behavior of microwave-assisted production of urchin-like and fiber-like CuO, as well as nanorods, which had shown the highest response towards NO_2 for urchin-like structures and

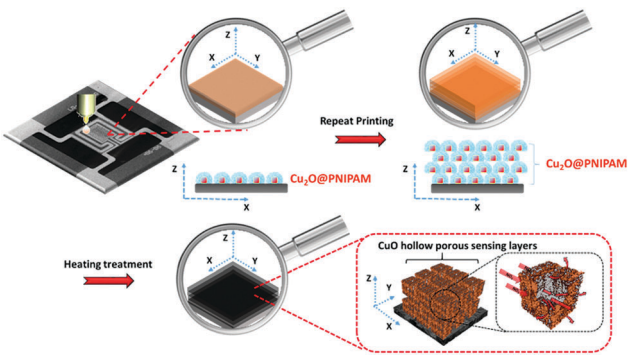

Scheme 1 Schematic illustration of the inkjet printing procedure used to fabricate a gas sensor device from Cu_2O@PNIPAM core–shell nanoparticles.

the fastest response for nanorods.[45] Previous work has also entailed a comparison of spherical and octahedral CuO[15] nanoparticles synthesized *via* precipitation reaction, porous cages using metal–organic frameworks as templates,[46] doped and undoped hollow spheres,[47] nanosheets[48] and nanoflowers apart from more traditional fabrication methods, such as sputtering.[49]

Experimental section

Materials and methods

Materials. Copper chloride ($CuCl_2$), sodium dodecyl sulfate (SDS), sodium hydroxide (NaOH), sodium ascorbate, poly(diallyldimethylammonium chloride) (20 wt% in H_2O) (PDDA), 4-styrenesulfonic acid sodium salt hydrate (NASS), *N*-isopropylacrylamide (NIPAM), and *N*,*N*′-methylene-bis-acrylamide (BIS) were supplied by Sigma-Aldrich. 2,2′-Azobis(2-methylpropionamidine dihydrochloride) (V50) was supplied by Fluka. All of the reactants were used without further purification. Water was purified by a Milli-Q system.

Synthesis of Cu_2O@PNIPAM core–shell nanoparticles. Similar to our previous work, the Cu_2O@PNIPAM core–shell nanoparticles can be synthesized in three steps (see Scheme 2).[41]

Firstly, Cu_2O nanocubes were synthesized by seed-mediated reaction method reported by Michael H. Huang's group[50] and washed by centrifugation. In the second step, Cu_2O nanocubes (0.66 mg mL^{-1}, 10 mL) were modified with NaSS (0.024 M, 10 mL) and PDDA (0.017 g mL^{-1}, 30 mL) as the interlayer. The unadsorbed PDDA and NaSS molecules can be removed by centrifugation (3500 rpm, 15 min) and the modified Cu_2O nanocubes were dispersed into 5 mL H_2O. With the help of double bonds supplied by the NaSS, the PNIPAM shells were successfully coated on the surface of Cu_2O nanocubes by precipitation polymerization by using V50 (0.018 M, 1 mL) as initiator at 75 °C. The polymerization was started immediately with the addition of 1 mL NIPAM (0.31 M) and BIS (9 mol% of NIPAM) into the mixture solution. The composite particles were then purified by centrifugation for several times and redispersed in water.

Inkjet printing. For inkjet deposition a Dimatix DMP-2831 printer system is used. Prior to the printing procedure, Cu_2O and Cu_2O@PNIPAM particle solutions are shortly redispersed using ultra sonic treatment for 30 s. 1 mL of the dispersion is transferred into the printer cartridge *via* a syringe and deposited onto MEMS sensing chips with a nozzle voltage of 37 ± 2 V, a droplet firing frequency of 2 kHz and a droplet pitch of 20 μm and a total area of 120 μm × 60 μm. The drop velocity is 34.3 m s^{-1} at a weight of 24 ng at a cartridge temperature of 26.6 °C and a platen temperature of 24.3 °C. Samples with varying amounts of superposed Cu_2O and Cu_2O@PNIPAM layers have been prepared, starting with a minimum of four stacked prints. The waveform used for jetting is shown in Fig. S1 (ESI†). The excess water substantially has been removed right after printing owing to quite small ink-drops deposited on the substrate and under the vacuum condition.

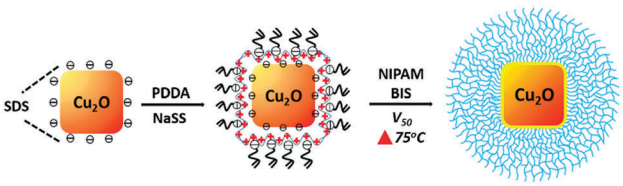

Scheme 2 Schematic illustration of the synthesis procedure of Cu_2O@PNIPAM core–shell nanoparticles.

Table 1 The relevant physical parameters and corresponding *Z* values of the bare Cu_2O nanocubes and Cu_2O@PNIPAM core–shell nanoparticles with different solid content at 20 °C (the diameter of the printing orifice is 25 μm)

Sample	Solid content (wt%)	Viscosity η (mPa s)	Density ρ (g cm^{-3})	Surface tension γ (mN m^{-1})	*Z* (Oh^{-1})
Cu_2O nanocubes	1.5	1.33	1.015	69.2	22.3
Cu_2O @PNIPAM	1.5	1.83	1.015	42.7	12.7
Cu_2O nanocubes	8	2.22	1.08	61	12.9

Evaluation of ink fluid properties. During the inkjet printing process, the relationship between fluid ink physical properties and the printability of the system can be represented by the inverse (*Z*) of the Ohnesorge number as the follows.[27,42]

$$Z = \frac{\sqrt{a\rho\gamma}}{\eta} = \mathrm{Oh}^{-1} \quad (1)$$

where *a* is the radius of the printing orifice (*a* = 12.5 μm in our experiment), ρ is the density of the ink, γ is the surface tension, and η is the viscosity (ρ, γ and η of the ink used in our experiment have been listed in Table 1). For different ink materials, the jettability range of *Z* is different. Normally the printable range of *Z* is considered within $1 < Z < 14$.[26,27] If the value of *Z* is too high, a large number of satellite droplets will be formed, whereas if it is too low, the ink will need more energy to form a new drop near the nozzle tip, which will prevent the separation of a drop.

Characterization

The hydrodynamic radius of the samples as a function of temperature was conducted by Zetasizer (Malvern Zetasizer Nano ZS ZEN 3500). Transmission electron microscope (TEM) images were done with JEOL JEM-2100 at 200 kV. X-ray diffraction (XRD) measurements were performed in a Bruker D8 diffractometer in the locked coupled mode (2θ ranging from 10° to 80°) with Cu $K\alpha_1$ radiation, the incident wavelength is 1.5406 Å. For the accomplished measurements the acceleration voltage is set to 40 kV and the filament current to 40 mA. The amount of Cu_2O in the Cu_2O@PNIPAM core–shell nanoparticles was determined by thermogravimetric analysis (TGA) using a Netsch STA 409PC LUXX. Fifteen milligrams of dried sample was heated to 800 °C under a constant argon flow (30 mL min^{-1}) with a heating rate of 10 K min^{-1}. Scanning electron microscope (SEM) measurements were done in a SEM LEO GEMINI 1530. Surface-tension was measured at room temperature by Contact Angle System OCA20 from dataphysics using pedant drop configuration. The size distribution of Cu_2O nanoparticles

was measured using Image J software based on the TEM images. Rheological measurements have been performed with a stress-controlled rheometer (Physica MCR 301, Anton Paar) equipped with cone-plate geometry (CP50). Shear steady tests were done with shear rate increased process from 10^{-3} to 10^{3} s^{-1} and the decreased process from 10^{3} to 10^{-3} s^{-1}. The surface morphology was investigated by atomic force microscope (AFM, Park System, XE – 100) operated in tapping mode using an etched Si tip with a tip radius of 10 nm with force constant of 40 N m^{-1}. All scans were performed on a scale of 40 μm × 40 μm with the lateral resolved height information on a square array of 256 × 256 pixels.

Gas sensitive characterization. The gas sensitive characterization was performed in a custom-made, fully automated measurement apparatus, which is described in detail in previous work.[51] The set-up allows for a characterization under varying trace gas concentrations, ambient background conditions, and surface temperatures. The Cu_2O sensing layers were deposited on low power MEMS devices[52] for electrical read-out of the Cu_2O sensing response and control of the layer's temperature.

Results and discussion

In our previous work,[41] we were able to modify Cu_2O nanocubes with thermosensitive PNIPAM shells by a two-step approach: the adsorption of an interlayer made up of PDDA and NaSS, and the coating by PNIPAM shells by precipitation polymerization. Due to the strong hydrophilic repulsion below the lower critical solution temperature (LCST) of PNIPAM, the modification of PNIPAM shell can significantly improve the colloidal stability of the Cu_2O nanocubes. Fig. 1a shows Cu_2O nanocubes without PNIPAM shells, from which aggregations can be clearly observed. Moreover, the photograph in Fig. S2 (ESI†) shows a coffee-ring shaped deposition on the substrate, which is a result of the aggregation of the nanoparticles along the periphery during drying process on a solid surface.[26,53] On the contrary, the coffee-ring disappeared after PNIPAM coating and a uniform film consisting of Cu_2O@PNIPAM core–shell nanoparticles was obtained, indicating homogeneous deposition of the particles.[26,35]

As shown in Fig. 1b, the Cu_2O@PNIPAM particles spontaneously formed an array of almost constant surface-to-surface distance after drying at room temperature on a Si wafer. The homogeneous deposition is essential to abstain the merging of adjacent particles and is critical to high-resolution inkjet printing patterns. Moreover, the homogeneous patterns and the cubic shapes of the particles were perfectly preserved after annealing at 350 °C under air, where the PNIPAM shell has been completely burned off and the Cu_2O nanoparticles have converted into CuO (Fig. 1c and Fig. S3, ESI†). The corresponding X-ray diffraction (XRD) patterns of the Cu_2O@PNIPAM core–shell nanoparticles before and after aerobic annealing are presented in Fig. 1d. The original Cu_2O signals disappeared completely after the high temperature treatment, while the peaks corresponding to the (110), (002) and (111) planes of CuO emerged according to the JCPDS card (No. 45-0937, red signals in Fig. 1d). This indicates that all of the Cu_2O nanoparticles have been transformed to CuO nanoparticles *via* the heating treatment. Fig. 2 shows the surface topographies of bare Cu_2O nanocubes and Cu_2O@PNIPAM core–shell nanoparticles on polystyrene (PS) substrate by drop-deposition, respectively. Without the modification of PNIPAM, most of the bare Cu_2O nanocubes were aggregated and cannot form a homogeneous thin coating as proved by AFM in Fig. 2a. Thus, parts of the substrate were not covered with nanoparticles. On the contrary, it can be observed from the AFM measurements that the thin film formed by the core–shell nanoparticles possessed much smoother surface and less average grain size than the one formed by the bare Cu_2O nanocubes. The root mean square (RMS) roughness obtained by the AFM scanning (40 μm × 40 μm) of the film formed from the core–shell microgels is 84.7 nm. This result further suggests that Cu_2O@PNIPAM core–shell nanoparticles can form very homogeneous patterns, which is critical to the high resolution pattern by inkjet printing and may be crucial in obtaining repeatable metal oxide based gas sensor fabrication.[19]

Apart from homogeneous deposition of the particles with patterned distribution and smoother surface, the PNIPAM

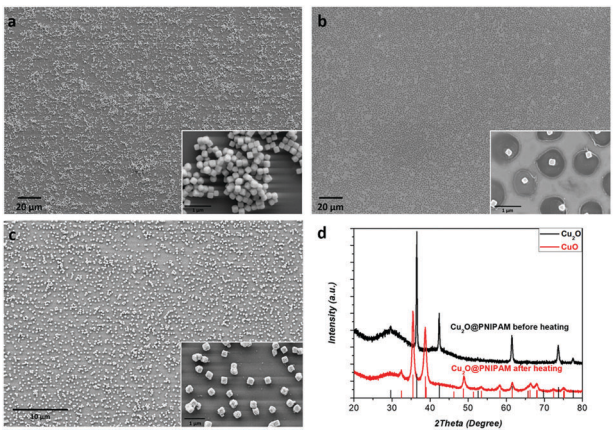

Fig. 1 SEM images of (a) Cu_2O nanocubes, Cu_2O@PNIPAM core–shell nanoparticles before (b) and after (c) heating treatment at 350 °C for 1 hour in the air; (d) XRD patterns of the Cu_2O@PNIPAM core–shell nanoparticles before (up) and after (below) heating treatment at 350 °C for 1 hour. As reference, standard XRD patterns of CuO (JCPDS: No. 45-0937) and Cu_2O (JCPDS: No. 65-3288) are shown in the plot.

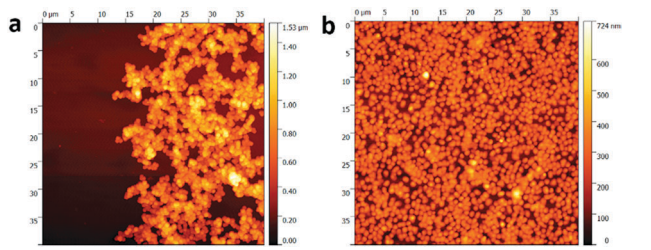

Fig. 2 AFM images of (a) the bare Cu_2O nanocubes and (b) the Cu_2O@PNIPAM core–shell nanoparticles drop deposited on PS substrates with the same solid content of 0.026 wt%.

shells significantly improved the stability of the ink system by forming an extremely stable dispersion. As shown in Fig. S4 (ESI†), the core–shell nanoparticles remained stable in water after storing overnight at room temperature without any visible sediment. Moreover, after being stored for 3 months, the ink solution can be redispersed homogeneously. On the contrary, without PNIPAM coating, an obvious precipitation has been observed for the bare Cu_2O nanocubes after 15 min and all of the particles precipitated at the bottom of the bottle overnight. Notably, with the protection of the PNIPAM shells, Cu_2O nanocubes can be effectively prevented from oxidation in water-based solutions for several months instead of a couple of weeks at the state of the art level. This property can greatly extend the shelf life of a Cu_2O aqueous solution as ink system.

As shown in Fig. 3, after storing in water in a dark place for 90 days, the cubic structure of the bare Cu_2O nanoparticles has been completely destroyed due to the oxidation into CuO, which can be also observed from the color change of the solution from orange to black (see the photo inset Fig. 3a and Fig. S4, ESI†). This is emphasized by the observation of new peaks at $2\theta = 35.5^\circ$, 38.8°, 48.6° and 58.4° corresponding to the Bragg reflections of CuO in the XRD patterns, which indicates the oxidation of bare Cu_2O nanocubes (Fig. 3c). In contrast, PNIPAM-modified nanocubes preserved all of the characteristic Cu_2O peaks and no other peaks were found in the XRD spectra after storing in water solution under the same condition for 90 days, indicating that none of the Cu_2O was oxidized (Fig. 3d). Moreover, all of the Cu_2O particles maintained their cubic structure and no aggregation was observed in the system (Fig. 3b).

The physical properties of fluid ink, like viscosity and surface tension, have a close relationship with the printability of the ink system and the resolution of the patterns. This relationship can be represented by the inverse (Z) of the Ohnesorge number as introduced previously. Only when the value of Z is within $1 < Z < 14$,[26,27] a high resolution pattern can be printed. The relevant physical parameters and corresponding Z values of the bare Cu_2O nanocubes and Cu_2O@PNIPAM core–shell nanoparticles with different solid content at 20 °C have been listed in Table 1. Due to the more uniform dispersion of the particles in water and the hydrophilicity exhibited by PNIPAM at room temperature, the Cu_2O sample with PNIPAM coating presents higher viscosity and lower surface tension than the bare one at the same solid content (1.5 wt%), which leads to a lower Z value in the printable range. While for the bare Cu_2O nanocubes, the Z value of the bare Cu_2O sample was adjusted within a reasonable range only when the solid content was increased from 1.5 wt% to 8 wt%. Moreover, as shown in Fig. S5 (ESI†), after being kept at room temperature for 30 min, the droplet of the bare Cu_2O nanocubes with solid content of 1.5 wt% became inhomogeneous and the upper portion of the droplet began depleted due to sedimentation. The above mentioned three dispersions were used to be printed on the devices (see Fig. S6, ESI†). Without introducing any additives, the device printed from pure Cu_2O dispersions with 1.5% solid content could not be uniformly covered by the nanoparticles and most of the device surface was bare. Thus, the Cu_2O@PNIPAM core–shell nanoparticle solution with solid content of 1.5 wt% and the pure Cu_2O nanocube solution with solid content of 8 wt% were used as the ink to prepare the gas sensor devices.

The Cu_2O@PNIPAM core–shell particles were printed on the interdigitated electrode structures of a micromachined hotplate device, resulting in the gas sensor elements which were subsequently characterized. Before the heating treatment, Cu_2O nanocubes were buried inside the PNIPAM shells to form a homogeneous layer (Fig. 4a). After an oxidizing treatment at 350 °C for one hour in the air, the PNIPAM shells were burned off resulting in a uniform layer of CuO nanocubes (Fig. 4b). The inset in Fig. 4b clearly shows that the CuO nanocubes are well separated from each other, no aggregation has been formed after heating treatment. In contrast, big islands of aggregations as well as numerous blank areas can be found on the surface of

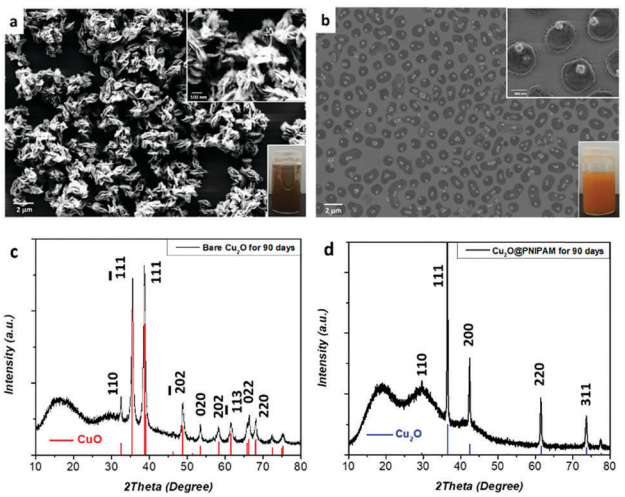

Fig. 3 SEM images of Cu_2O nanocubes without (a) and with (b) PNIPAM coating after 90 days' storage in aqueous solution; XRD patterns of (c) bare Cu_2O nanocubes kept in water at room temperature for 90 days and (d) Cu_2O@PNIPAM core–shell nanoparticles with the same treatment.

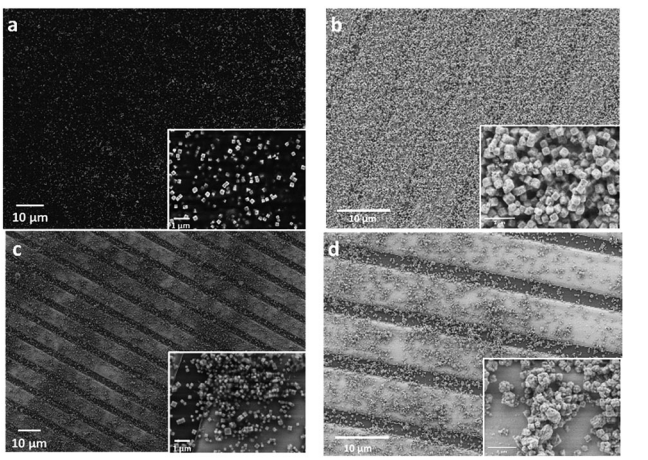

Fig. 4 (a and b) SEM images of gas sensor devices of Cu_2O@PNIPAM core–shell nanoparticles before and after heating treatment. (c and d) SEM images of gas sensor device of pure Cu_2O nanocubes before and after heating treatment.

the device (Fig. 4c). After the oxidization treatment, the cubic structures were totally destroyed by sintering, large yet sparser and random bulky particles were found as shown in the inset of Fig. 4d.

Most importantly, the thermal treatment not only transforms Cu_2O to CuO, but also facilitates the formation of hollow porous CuO nanocubes (as shown in Fig. S7, ESI†). Compared to dense particles, hollow, porous nanostructures favor higher sensitivity stemming from the large surface-to-volume ratio, high specific surface area, more surface active sites as well as the effect of crystal facets with high surface reactivity.[54]

In order to understand the conversion process from Cu_2O@PNIPAM core–shell nanoparticles to CuO hollow porous nanocubes, TEM images were taken for the samples at different stages of processing. Fig. 5a shows a TEM image of a zoomed single Cu_2O@PNIPAM nanoparticle at room temperature, where the PNIPAM shell with low contrast and Cu_2O nanocube with a smooth surface can be observed. Since the thermal decomposition of PNIPAM started from 320 °C (see the TGA curve of Cu_2O@PNIPAM nanoparticles in Fig. S3, ESI†), the contrast of Cu_2O nanocube became more clearly due to the burning of the PNIPAM shell after pyrolysis in air for 5 min. Moreover, a very thin layer of rough CuO crystal, which contained much weaker contrast than Cu_2O, was found around the surface of the nanocube (shown in Fig. 5b and the corresponding 3D model below). As can be seen in Fig. 5c and d, continuous heating of the particles at 350 °C for 60 min resulted in a gradually clear hollow porous structure of the nanocubes. This suggests that the conversion of Cu_2O to CuO started from the surface of the nanocubes and then migrated from the inner part during the oxidation process according to the Ostwald ripening.[28] Thus, it is believed that the PNIPAM shells assist the preservation of the original shape of the nanocubes in the initial oxidation stage before being burned off, thus playing a crucial role in the formation of the hollow cubic nanostructures of CuO.

Fig. 6a shows the sensing response of two exemplary CuO gas sensor devices prepared by using bare Cu_2O nanocubes and Cu_2O@PNIPAM core–shell nanoparticles, respectively. The sensors were operated at a typical elevated temperature of 300 °C and exposed to varying levels of 1–10 ppm NO_2 in dry synthetic air. Both of the devices show a typical p-type sensing behavior with respect to the oxidizing nature of NO_2 and the given temperature. The baseline resistance is distinctly below the MΩ range, which is favorable for dedicated circuitry. This can be explained with the regular and ordered intra-particle arrangement and the porous hollow nanostructures, which promotes the current flow. On the contrary, the bare nanoscale particles aggregate into larger clusters yet sparser and random bulky particles during the heating treatment, resulting in a higher baseline resistance. The highly homogeneous deposition of the Cu_2O@PNIPAM particles may also point towards a method to improve the repeatability of metal oxide based gas sensors.[19] The experiments were conducted at different operation temperatures as well. Fig. 6b shows the mean response characteristics of the device prepared from core–shell nanoparticles in a log–log representation for different operational temperatures. The response is here defined as the ratio of the baseline resistance in dry synthetic air (R_0) and the resistance upon NO_2 exposure (R). The sensing elements made from the core–shell nanoparticles show a thermal behavior consistent with other CuO morphologies at operating temperatures of 250 °C, 300 °C, and 350 °C, respectively.[55] The results reveal a significant temperature dependence in sensitivity in line with the expected behavior of CuO sensing layers. The device made from core–shell nanoparticles, which formed hollow porous nanocubes layer, feature a faster response and recovery characteristic upon alternating NO_2 exposure and purging with synthetic air.

As a measure for the response time we determine the time t_{90} it takes to achieve 90% of the new steady state value upon a change in the gas matrix. For the reaction of the functional layer towards NO_2 and for recovering the baseline after removal of NO_2 the Cu_2O@PNIPAM nanoparticle derived layers are about 40% faster. While the bare Cu_2O nanocube layers on average need $t_{90,ads}$ = 21.5 min for reacting to NO_2 and $t_{90,des}$ = 91.9 min for recovering the baseline, the Cu_2O@PNIPAM layer achieve $t_{90,ads}$ = 12.6 min and $t_{90,des}$ = 55.6 min, respectively.

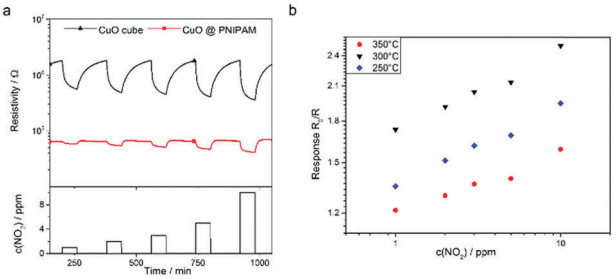

Fig. 6 (a) Comparison of the sensing characteristics of bare CuO nanocubes (Ink solid content: 8 wt%) and CuO nanocubes from Cu_2O@PNIPAM core–shell nanoparticles (ink solid content: 1.5 wt%) gas sensors towards increasing NO_2 levels in dry synthetic air and an operating temperature of 300 °C. (b) Response characteristics of core–shell nanoparticle sensing devices for operation temperatures of 250 °C, 300 °C, and 350 °C respectively, which can be described by a typical power-law and reveal a distinct temperature dependency of sensitivity.

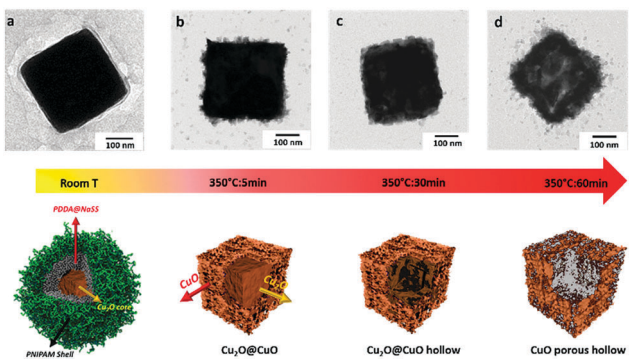

Fig. 5 TEM images of Cu_2O@PNIPAM core–shell nanoparticle (a) at room temperature, after heating at 350 °C (b) for 5 min, (c) for 30 min and (d) for 60 min. The scale bars shown in the TEM images were 100 nm.

Conclusions

In conclusion, the facile fabrication of CuO-based gas sensor with low material consumption and high sensitivity has been demonstrated by utilizing the Cu_2O@PNIPAM core–shell microgels as novel ink system. The PNIPAM shell plays an essential role in the quest for the formation of uniform sensing layers and porous nanostructures. Firstly, the Cu_2O@PNIPAM core–shell microgel dispersion shows significant improvement in colloidal stability and fluid properties compared with the native Cu_2O nanocubes at room temperature. Thus, the aqueous dispersion of Cu_2O@PNIPAM core–shell nanoparticles with low solid content (1.5 wt%) can be used directly as ink materials for the high resolution inkjet printing without introducing any other surfactants and organic solvents. Secondly, due to the protection of the PNIPAM shell, the uniform distribution of CuO nanoparticles can be preserved without merging into large aggregations after heating treatment. Gas sensing layers composed of hollow porous CuO nanocubes can be obtained after heat treatment at 350 °C for 60 min from the core–shell nanoparticles, which resulted in more sensitive gas sensor device. The remarkable improvements on high sensitivity and dodge of material wasting lie in the innovation strategy of modifying Cu_2O nanocubes with PNIPAM shell, which can be extended to various inorganic nanomaterials.

Conflicts of interest

There are no conflicts to declare.

Acknowledgements

H. J. gratefully acknowledges financial support of the CSC scholarship. S. P. acknowledges funding from the Community of Madrid under grant number 2016-T1/AMB-1695. We also thank Dr Miriam Siebenbürger for her kind help for the rheological measurements and Prof. Jiayin Yuan for his professional suggestions about the modification of the manuscript.

References

1 C. Wang, L. Yin, L. Zhang, D. Xiang and R. Gao, *Sensors*, 2010, **10**, 2088–2106.
2 J.-K. Sun and Q. Xu, *Energy Environ. Sci.*, 2014, **7**, 2071.
3 X. Liu, T. Ma, N. Pinna and J. Zhang, *Adv. Funct. Mater.*, 2017, **27**, 1–30.
4 F. Wang, H. Li, Z. Yuan, Y. Sun, F. Chang, H. Deng, L. Xie and H. Li, *RSC Adv.*, 2016, **6**, 79343–79349.
5 J. Liu and D. Xue, *Adv. Mater.*, 2008, **20**, 2622–2627.
6 J. Zhang, X. Liu, G. Neri and N. Pinna, *Adv. Mater.*, 2016, **28**, 795–831.
7 Y. Sui, Y. Zeng, L. Fu, W. Zheng, D. Li, B. Liu and B. Zou, *RSC Adv.*, 2013, **3**, 18651.
8 W. C. Huang, L. M. Lyu, Y. C. Yang and M. H. Huang, *J. Am. Chem. Soc.*, 2012, **134**, 1261–1267.
9 C. G. Morales-Guio, S. D. Tilley, H. Vrubel, M. Grätzel and X. Hu, *Nat. Commun.*, 2014, **5**, 3059.
10 C.-Y. Lin, Y.-H. Lai, D. Mersch and E. Reisner, *Chem. Sci.*, 2012, **3**, 3482.
11 K. Chen, S. Song and D. Xue, *CrystEngComm*, 2015, **17**, 2110–2117.
12 J. C. Park, J. Kim, H. Kwon and H. Song, *Adv. Mater.*, 2009, **21**, 803–807.
13 T. Jiang, T. Xie, W. Yang, H. Fan and D. Wang, *J. Colloid Interface Sci.*, 2013, **405**, 242–248.
14 J. Zhang, J. Liu, Q. Peng, X. Wang and Y. Li, *Chem. Mater.*, 2006, **18**, 867–871.
15 K. Henzler, A. Heilemann, J. Kneer, P. Guttmann, H. Jia, E. Bartsch, Y. Lu and S. Palzer, *Sci. Rep.*, 2015, **5**, 17729.
16 J. Kneer, J. Wöllenstein and S. Palzer, *Appl. Phys. Lett.*, 2014, 105.
17 J. Kneer, S. Knobelspies, B. Bierer, J. Wöllenstein and S. Palzer, *Sens. Actuators, B*, 2016, **222**, 625–631.
18 N. B. Tanvir, O. Yurchenko, C. Wilbertz and G. Urban, *J. Mater. Chem. A*, 2016, **4**, 5294–5302.
19 H. Gao, H. Jia, B. Bierer, J. Wöllenstein, Y. Lu and S. Palzer, *Sens. Actuators, B*, 2017, **249**, 639–646.
20 A. Chowdhuri, V. Gupta, K. Sreenivas, R. Kumar, S. Mozumdar and P. K. Patanjali, *Appl. Phys. Lett.*, 2004, **84**, 1180–1182.
21 K. Sahner and H. L. Tuller, *J. Electroceram.*, 2010, **24**, 177–199.
22 J. Li, S. Sollami Delekta, P. Zhang, S. Yang, M. R. Lohe, X. Zhuang, X. Feng and M. Östling, *ACS Nano*, 2017, **11**, 8249–8256.
23 W. Shen, X. Zhang, Q. Huang, Q. Xu and W. Song, *Nanoscale*, 2014, **6**, 1622–1628.
24 N. Marjanovic, J. Hammerschmidt, J. Perelaer, S. Farnsworth, I. Rawson, M. Kus, E. Yenel, S. Tilki, U. S. Schubert and R. R. Baumann, *J. Mater. Chem.*, 2011, **21**, 13634.
25 H. O. Thomas Oehlund, Anna K. Schuppert, Magnus Hummelgard, Joakim Baeckstroem and Hans-Erik Nilsson, *ACS Appl. Mater. Interfaces*, 2015, **7**, 18273–18282.
26 F. Torrisi, T. Hasan, W. Wu, Z. Sun, A. Lombardo, T. S. Kulmala, G.-W. Hsieh, S. Jung, F. Bonaccorso, P. J. Paul, D. Chu and A. C. Ferrari, *ACS Nano*, 2012, **6**, 2992–3006.
27 D. Jang, D. Kim and J. Moon, *Langmuir*, 2009, **25**, 2629–2635.
28 W. Lee, Y. S. Lim, S. Kim, J. Jung, Y.-K. Han, S. Yoon, L. Piao and S.-H. Kim, *J. Mater. Chem.*, 2011, **21**, 6928.
29 H. S. Lee and M. Y. Yang, *IEEE Trans. Device Mater. Reliab.*, 2016, **16**, 604–609.
30 T. T. Baby, S. K. Garlapati, S. Dehm, M. Ha, R. Kruk and H. Hahn, *ACS Nano*, 2015, 3075–3083.
31 Y. X. Wang, X. F. Tang and Z. G. Yang, *Colloids Surf., A*, 2011, **388**, 38–40.
32 Z. Meng, J. K. Cho, V. Breedveld and L. A. Lyon, *J. Phys. Chem. B*, 2009, **113**, 4590–4599.
33 Y. Lu and M. Drechsler, *Langmuir*, 2009, **25**, 13100–13105.
34 M. Takizawa, Y. Sazuka, K. Horigome, Y. Sakurai, S. Matsui, H. Minato, T. Kureha and D. Suzuki, *Langmuir*, 2018, **34**, 4515–4525.
35 K. Horigome and D. Suzuki, *Langmuir*, 2012, **28**, 12962–12970.

36 B. Wedel, Y. Hertle, O. Wrede, J. Bookhold and T. Hellweg, *Polymers*, 2016, **8**, 162.
37 T. Hellweg, *J. Polym. Sci., Part B: Polym. Phys.*, 2013, **51**, 1073–1083.
38 A. Balaceanu, Y. Verkh, D. Kehren, W. Tillmann and A. Pich, *Z. Phys. Chem.*, 2014, **228**, 253–267.
39 J. Pérez-Juste, I. Pastoriza-Santos and L. M. Liz-Marzán, *J. Mater. Chem. A*, 2013, 20–26.
40 S. Jaber, M. Karg, A. Morfa and P. Mulvaney, *Phys. Chem. Chem. Phys.*, 2011, **13**, 5576–5578.
41 H. Jia, R. Roa, S. Angioletti-Uberti, K. Henzler, A. Ott, X. Lin, J. Möser, Z. Kochovski, A. Schnegg, J. Dzubiella, M. Ballauff and Y. Lu, *J. Mater. Chem. A*, 2016, **4**, 9677.
42 J. E. Fromm, *IBM J. Res. Dev.*, 1984, **28**, 322–333.
43 A. Loutfi, S. Coradeschi, G. K. Mani, P. Shankar and J. B. B. Rayappan, *J. Food Eng.*, 2015, **144**, 103–111.
44 A. D'Amico, G. Pennazza, M. Santonico, E. Martinelli, C. Roscioni, G. Galluccio, R. Paolesse and C. Di Natale, *Lung Cancer*, 2010, **68**, 170–176.
45 D. P. Volanti, A. A. Felix, M. O. Orlandi, G. Whitfield, D. J. Yang, E. Longo, H. L. Tuller and J. A. Varela, *Adv. Funct. Mater.*, 2013, **23**, 1759–1766.
46 Y. Wang, Y. Lü, W. Zhan, Z. Xie, Q. Kuang and L. Zheng, *J. Mater. Chem. A*, 2015, **3**, 12796–12803.
47 Y. H. Choi, D. H. Kim and S. H. Hong, *Sens. Actuators, B*, 2017, **243**, 262–270.
48 A. Umar, A. A. Alshahrani, H. Algarni and R. Kumar, *Sens. Actuators, B*, 2017, **250**, 24–31.
49 P. Samarasekara, N. T. R. N. Kumara and N. U. S. Yapa, *J. Phys.: Condens. Matter*, 2006, **18**, 2417–2420.
50 C. H. Kuo, C. H. Chen and M. H. Huang, *Adv. Funct. Mater.*, 2007, **17**, 3773–3780.
51 J. Kneer, A. Eberhardt, P. Walden, A. Ortiz Pérez, J. Wöllenstein and S. Palzer, *Rev. Sci. Instrum.*, 2014, **85**, 055006.
52 P. Walden, J. Kneer, S. Knobelspies, W. Kronast, U. Mescheder and S. Palzer, *J. Microelectromech. Syst.*, 2015, **24**, 1384–1390.
53 R. D. Deegan, O. Bakajin, T. F. Dupont, G. Huber, S. R. Nagel and T. A. Witten, *Nature*, 1997, **389**, 827–829.
54 M. R. Alenezi, S. J. Henley, N. G. Emerson and S. R. P. Silva, *Nanoscale*, 2014, **6**, 235–247.
55 J. Kneer, S. Knobelspies, B. Bierer, J. Wöllenstein and S. Palzer, *Sens. Actuators, B*, 2016, **229**, 57–62.